Applied Surface Science 410 (2017) 315–325

Contents lists available at ScienceDirect

Applied Surface Science

journal homepage: www.elsevier.com/locate/apsusc

Full Length Article

Microwave-assisted nitric acid treatment of sepiolite and functionalization with polyethylenimine applied to CO_2 capture and CO_2/N_2 separation

E. Vilarrasa-García[a], J.A. Cecilia[b,*], M. Bastos-Neto[a], C.L. Cavalcante Jr.[a], D.C.S. Azevedo[a,*], E. Rodríguez-Castellón[b]

[a] Department of Chemical Engineering, Universidade Federal do Ceará, Campus do Pici, bl. 709, 60455-760 Fortaleza, Brazil
[b] Department of Inorganic Chemistry, Cristallography and Mineralogy, Universidad de Málaga, Campus de Teatinos s/n, 29071 Málaga, Spain

ARTICLE INFO

Article history:
Received 14 November 2016
Received in revised form 8 February 2017
Accepted 6 March 2017
Available online 8 March 2017

Keywords:
Sepiolite
Polyethylenimine
Microwave radiation
CO_2 adsorption
Equilibrium
CO_2/N_2 selectivity

ABSTRACT

Sepiolite was treated in HNO_3 solutions with the assistance of microwave radiation. This treatment caused the progressive depletion of Mg^{2+}, the gradual degradation of the sepiolite structure and the formation of an amorphous silica phase, which contributes to a noticeable increase of the surface area. The use of microwaves during acid treatment, after few minutes, led to materials with similar S_{BET} to those obtained after 48 h with conventional heating methods. The influence of mineralogical impurities, crystallinity and chemical composition in the reactivity of sepiolite to this treatment was also studied. The obtained materials were impregnated with polyethylenimine and assessed for CO_2 capture and CO_2/N_2 selectivity at different temperatures. Experimental equilibrium data were fitted to Langmuir and Sips models. The adsorption data revealed that sepiolite can be an interesting adsorbent for CO_2 capture, achieving a capacity of 1.70 mmol g^{-1} at 338 K and 1 bar, providing a high CO_2/N_2 selectivity (440 mol CO_2/mol N_2).

1. Introduction

The world industrialization in the last two centuries has been pointed as the main cause of the gradual warming of the Earth due to the increasing emissions of the so-called greenhouse gases. Among these gases, carbon dioxide (CO_2) has reached levels higher than 400 ppm today [1], which is believed to be the major cause of climate change. The Intergovernmental Panel on Climate Change (IPCC) states that the world average temperature has been rising in the past 100 years and an increase of ca. 6–8% is to be expected by the end of the twenty-first century [2].

Global warming is claimed to be the cause of droughts, floods, heat waves, destruction of ecosystems as well as economic losses. Hence, global society has been urged to discuss and develop more stringent environmental laws and regulations in order to minimize CO_2 emissions originated from the combustion of fossil fuels.

In this context, new effective methods for the capture and sequestration of CO_2 from post-combustion effluents have been developed in the last decades. The main technologies have been focused on cryogenic distillation, membrane purification, absorption with liquids and adsorption using solids [3]. Cryogenic distillation is an efficient process where the components are separated by a series of compression, cooling and expansion steps, although its application is limited due to its high energy demand. Membranes are also widely used in gas separation; however its efficiency tends to be low when the gas mixture is poor in CO_2. CO_2 absorption with liquids is the main large-scale CO_2 capture technology using solvents with basic character such as alkyl amine solutions. Nevertheless, this process shows drawbacks due to the low thermal stability and consequent degradation of the amine-based compounds, which leads to reduced effectiveness and equipment corrosion. Moreover, this method requires relatively high energy consumption for solvent regeneration [4,5]. Adsorption in porous media is an alternative method to capture CO_2, although further development of adsorbents is still necessary for its use in relatively concentrated streams.

The process of capturing CO_2 using a dry adsorbent involves the selective storage and separation of CO_2 based on gas–solid interactions [6]. Several parameters, such as surface chemistry and pore

* Corresponding authors.
E-mail addresses: enrique@gpsa.ufc.br (E. Vilarrasa-García), jacecilia@uma.es (J.A. Cecilia), mbn@ufc.br (M. Bastos-Neto), celio@gpsa.ufc.br (C.L. Cavalcante Jr.), diana@gpsa.ufc.br, diana@pq.cnpq.br (D.C.S. Azevedo), castellon@uma.es (E. Rodríguez-Castellón).

http://dx.doi.org/10.1016/j.apsusc.2017.03.054
0169-4332/

size of the adsorbent as well as the operating conditions (i.e. temperature and partial pressure), are key factors in the capture process [7].

Cyclic adsorption processes are classified according to the regeneration step and the usual configurations are: a)pressure swing adsorption (PSA) [8,9]; b) temperature-pressure-swing adsorption (TPSA) [10,11], where two processes are combined, i.e., adsorption at a low temperature followed by desorption/regeneration by heating and lowering the pressure; c) electric-swing adsorption (ESA) [12], i.e., adsorption/desorption by varying the electricity supply, with a low-voltage current passing through the adsorbent; and d) vacuum swing adsorption (VSA) [13]. Furthermore, adsorption-based technologies such as pressure/vacuum-swing adsorption (PVSA) have been frequently investigated because of their potentially low energy requirements and relative simplicity [14,15]. The use of commercially available adsorbents, as zeolites and carbons, is well known. These adsorbents preferentially bind CO_2 either by weak van der Waals forces or, for instance, by stronger dipole–quadrupole (electrostatic) interactions between CO_2 and alkali-metal cations in the zeolite frameworks [16]. The adsorption efficiency is thought to be improved and stabilized by modifying the surface of the adsorbent material with amine groups, which display high affinity towards CO_2. However, the functionalization caused by the incorporation of amine groups is not always beneficial because it may impair diffusion, particularly in materials with smaller pore size.

Silica-based mesoporous materials have been widely evaluated for the CO_2 capture. Thus, adsorbents such as SBA-15 [17–21], MCM-41 [22], HMS [23,24], KIT-6 [25] or mesocellular silica foams have been studied due to their high surface area, adequate size of the mesochannels [19,20] for amine functionalization and high thermal and mechanical resistances. The incorporation of amine groups on the mesoporous materials enhances the CO_2 capture efficiency. These functionalization procedures are carried out following two main strategies. The first strategy is based on a grafting process between the silanol groups located on the surface of the adsorbent and aminosilane species, leading to adsorbents with high thermal stability, high water tolerance and high selectivity towards CO_2 [17]. The second strategy is based on the impregnation of porous silica with large amounts of amine polymers (e.g., polyethyleneimine or PEI and tetraethylenepentamine or TEPA); where the amine polymer is stabilized by hydrogen bonding with surface silanol groups, although CO_2 adsorption is restricted by diffusional considerations [18,26].

Metal organic framework adsorbents display a structure with large body volume because the pores are attached to organic molecules and knots of metallic ions. MOFs are widely used as storage media for various gases because the pore diameters can be easily controlled [27,28]. However MOFs have poor performance as compared to other solid sorbents at low partial pressures of CO_2, and maintenance of a high partial pressure is not always economically feasible. In addition, MOFs are complex, expensive and suffer from hydrothermal and mechanical unstabilities.

Metal oxides such as CaO and MgO are candidates for CO_2 capture because of their basicity, low cost, low toxicity and high availability. However, the regeneration of these materials requires high-energy consumption rendering this process relatively expensive [29].

Most of the adsorbents reported in the literature are not commercially available for full-scale industrial operation. Thus, it is necessary to develop low-cost materials with high thermal, chemical and mechanical stability to be used as adsorbents for CO_2 capture from the fossil fuel-fired power plants with high selectivity towards CO_2 in comparison to other flue gases, such as N_2. With this respect, clay minerals are the most abundant inorganic component on the surface of the Earth. Several phyllosilicates such as kaolinite [30,31], bentonite [30–33] or sepiolite [34] have been modified by acid treatment to improve their textural properties by partial digestion of the clay mineral structure.

The aim of the present work is to evaluate the adsorption capacity for CO_2 of sepiolites modified by a microwave-assisted acid treatment. The use of microwave-heating techniques in the acid activation of clay minerals offers advantages over conventional methods including a higher heating rate that reduces the treatment time and promoteshomogeneous heating [35–37]. The treated sepiolites were impregnated with polyethylenimine (PEI), a rich-amine polymer. The influence of the activation time of the sepiolite as well as the amount of loaded amine of PEI were evaluated in this work. Moreover, in order to assess the adsorption capacity of these materials in flue gas of power plants, CO_2 adsorption in presence of N_2 was also studied.

2. Experimental

2.1. Materials

The starting material was a sepiolite obtained from Madrid Basin deposits (Barajas, Madrid, Spain). The reagent used in the acid treatment was nitric acid (HNO_3, VWR 68%). The impregnation of the activated sepiolite was performed with branched polyethylenimine (PEI) (average molecular weight Mn ~600, Aldrich) using methanol 99.9% (Aldrich) as solvent. He (Air Liquide 99.99%), N_2 (Air Liquide 99.9999%) and CO_2 (Air Liquide 99.998%) were employed for measurements on the manometric equipment (up to 1 bar). For CO_2 and N_2 adsorption measurements at high pressure White Martins supplied CO_2 (99.5%) and N_2 (99.990%).

2.2. Preparation of the adsorbents

In each acid activation process, about 5 g of dried sepiolite were treated with 50 mL of 0.2 mol L^{-1} HNO_3 for 2, 4, 8 and 16 min under microwave radiation at 800 W, in an open glass cylinder reactor. Franco and coworkers [35] compared in their research the use of two different acid solutions (HNO_3 and HCl with the same concentration) and concluded that the use of HNO_3 was more effective in terms of increasing textural properties in the range of treatment time under study.

After the acid treatment, the samples were washed until a neutral pH was reached and then centrifuged. Then, samples were dried at 333 K overnight. The obtained samples were labeled according to the treatment time as follows: S (non-treated), S-2 m, S-4 m, S-8 m and S-16 m for 0, 2, 4, 8 and 16 min under microwave radiation, respectively. Then, the samples were impregnated with a PEI loading in the range of 20–60 wt.%, as described elsewhere [18,20].

2.3. Characterization techniques

The chemical analysis (major elements) of untreated samples and obtained products was performed by means of the MagiX X-ray fluorescence (XRF) spectrometer of PANanalytical.

X-ray diffraction (XRD) was used to identify the crystalline phases of the synthesized solids. These experiments were performed on an X'Pert Pro MPD automated diffractometer equipped with a Ge (111) primary monochromator (strictly monochromatic Cu-Kα radiation) and an X'Celerator detector. Measurements were obtained for 2θ in the range of 2–65°.

The textural parameters (S_{BET}, V_P and D_P) were evaluated from nitrogen adsorption-desorption isotherms at 77 K as determined by an automatic ASAP 2020 system from Micromeritics. Prior to the measurements, samples were outgassed at 473 K and 10^{-4} mbar overnight. Specific surface areas were determined by using the Brunauer–Emmett–Teller (BET) equation [38] assuming a cross

section of 0.162 nm^2 for the nitrogen molecule. Micropore surface areas were obtained by de Boer's t-plot method [39]. The specific pore volume was calculated by applying the Barrett-Joyner-Halenda (BJH) method [40] to the desorption branch of the N_2 isotherm. The total pore volume was calculated from the total N_2 adsorbed at a relative pressure of 0.996.

FTIR spectra were collected on a Varian 3100 FTIR spectrophotometer. The interferograms consisted of 200 scans, and the spectra were collected using a KBr spectrum as background. About 30 mg of a mixture of each sample and KBr with a weight ratio of 1:9 were placed in the sample holder and then spectra were collected.

Elemental chemical analysis was performed with a LECO CHNS 932 analyzer to determine the nitrogen content present through the combustion of the samples at 1373 K in pure oxygen to form NO_x.

For the acid treatment, a commercially available microwave system EMS20100OX (Electrolux, Sweden) operating at 800 W and 2.445 GHz was used. In all cases, the irradiation was supplied in discontinuous form, pausing every minute, to avoid that the suspension temperature exceeds 373 K [41].

2.4. CO_2 adsorption test

CO_2 adsorption-desorption isotherms were measured with a Micromeritics ASAP 2020 Analyzer (i.e., by volumetry-manometry) at 298, 318 and 338 K. Prior to the measurements, samples were outgassed at 473 K and 10^{-4} mbar overnight.

Single gas CO_2, N_2 and binary mixture gas CO_2/N_2 adsorption measurements at higher pressure were performed using a Rubotherm (Bochum, Germany) magnetic suspension balance equipped with a gas mixture dosing unit. Around 0.5 g of each sample were used for gravimetric measurements. Prior to each measurement, samples were outgassed at 473 K for 2 h (heating rate of 2 K min^{-1}) under vacuum (10^{-3} bar). The regenerated samples were exposed to stepwise increases of the pure (or mixed) gas pressure at constant temperature. The change in weight of the samples after each pressure step was measured continuously until equilibrium was reached. The condition to satisfy equilibrium was a mass variation of less than 10^{-4} g for 30 min. A correction for the buoyancy effect was performed by helium gas measurements at 298 K in the pressure range of 0–12 bar, to allow for determination of the excess adsorbed concentration. The temperature during the adsorption isotherms measurements was held constant by means of a thermostat bath.

The excess adsorbed concentration (g or mol of adsorbate gas per unit mass of adsorbent) was calculated by application of Eq. (1):

$$m_{exc} = \Delta m + \rho (V_b + V_s) \quad (1)$$

where m_{exc} is the excess adsorbed concentration, Δm is the mass difference (per unit mass of adsorbent) between the mass at each pressure and the mass under vacuum (after regeneration), ρ is the density (at a fixed P and T) of the gas surrounding the adsorbent. Density was obtained in either two ways: from equations of state (CO_2 ([42]), N_2 ([43]), He ([44]) or experimentally by direct measurements using the balance. V_s and V_b are the specific volumes of adsorbent solid phase and suspended components inside the measuring chamber, respectively.

Isotherms were obtained in the pressure range of 0–10 bar. Within this range the deviations between excess adsorbed concentration and absolute adsorbed concentration for CO_2 and N_2 are negligible [45] and hence no correction to the experimental values (excess adsorbed concentration ~ absolute adsorbed concentration) were required for the sake of comparison with predictive equilibrium models.

2.5. Equilibrium models

The simplest theoretical model for monolayer adsorption is the Langmuir model. The Langmuir adsorption model is still the most widely used procedure to fit pure gas isotherms. The Langmuir equation is

$$q = q_m \frac{bP}{1 + bP} \quad (2)$$

where q is the quantity of gas adsorbed per unit mass of adsorbent at a given T and P, q_m is the maximum adsorbed concentration in mmol g^{-1} [46]. Parameter b is related to the affinity between adsorbate and adsorbent (Langmuir constant), which defines the strength of the adsorbate-adsorbent interaction. When the affinity constant b is larger, the adsorbate molecule is more strongly bound to the adsorbent surface as a result of the stronger affinity of adsorbate molecule with the surface of the adsorbent. Besides, an increase in temperature decreases the amount adsorbed at a given pressure due to the higher energy needed for the adsorbed molecule to evaporate [47]. Eq. (3) is used to describe the relation between the b parameter and temperature:

$$b = b_0 e^{E_a/RT} \quad (3)$$

where b_0 and E_a are constant parameters for the pair adsorbent-adsorbate, and they are defined as pre-exponential factor and activation energy, respectively.

Another model applied to represent the experimental data was the Sips model (Eq. (4)).

$$q = q_m \frac{(bP)^{1/m}}{1 + (bP)^{1/m}} \quad (4)$$

The difference between this equation in comparison to the Langmuir equation is the incorporation of parameter "m" that defines the heterogeneity of the system. Thus, when this parameter is equal to the unity, the Sips equation reduces to the Langmuir equation, which can be applied for ideal surfaces. Nonetheless, the parameter m is usually greater than unity, and therefore the larger this parameter, the more heterogeneous the system is [47].

Another model used to fit the pure component experimental data was the single gas Dualsite Sips model ($q_{m1}, b_1, m_1, q_{m2}, b_2, m_2$). This model assumes that the solid is mainly composed of two energetically different adsorption sites. All assumptions of the Langmuir model can be applied to each site, with no interactions between the two different sites, so that the total adsorbed concentration would be given by Eq. (5):

$$q = q_{m1} \frac{(b_1 P)^{1/m_1}}{1 + (b_1 P)^{1/m_1}} + q_{m2} \frac{(b_2 P)^{1/m_2}}{1 + (b_2 P)^{1/m_2}} \quad (5)$$

where q is the adsorbed concentration of adsorbate gas (mmol g^{-1}) in equilibrium with adsorbate pressure (e.g. mmHg), whereas q_{m1} and q_{m2} are the saturation capacities for sites 1 and 2, respectively; and b_1 and b_2 are the affinity parameters for site 1 and 2, respectively. In this work, it has been assumed that site 1 is related to non-specific physisorption between the solid and the gas molecules, whereas site 2 is associated with CO_2 adsorption by reaction with amino groups and on this site only CO_2 is adsorbed.

Multicomponent adsorption equilibria may often be predicted from single-gas component data. Therefore, successful prediction of multicomponent adsorption equilibria strongly relies on accurate measurements of single component data and on a precise correlation of these data with an isotherm model for mixtures. In this work, we have tried to predict the amount adsorbed of component i of a binary mixture by applying the following models:

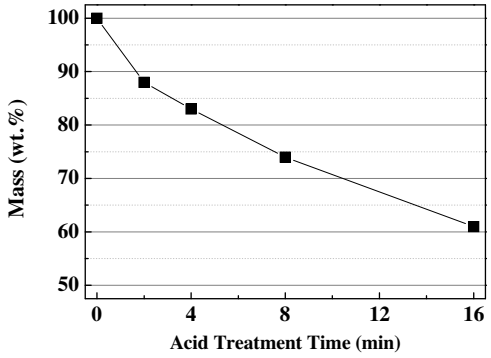

Fig. 1. Percent mass of samples with respect to the pristine sepiolite (100%) as a function of time of microwave assisted acid treatment.

Extended Langmuir (Eq. (6)), Extended Sips (Eq. (7)) and Extended Dualsite Langmuir (Eq. (8)) and Sips (Eq. (9)).

$$q = \frac{q_{m,i} b_i P_i}{1 + (\sum_{i=1}^{N} b_i P_i)} \tag{6}$$

$$q = \frac{q_{m,i} (b_i P_i)^{1/m_i}}{1 + (\sum_{i=1}^{N} b_i P_i)^{1/m_i}} \tag{7}$$

$$q = \frac{q_i b_i P_i}{1 + b_i P_i} + \frac{q_j b_j P_j}{1 + (\sum_{j=1}^{N} b_j P_j)} \tag{8}$$

$$q = \frac{q_i (b_i P_i)^{1/m_i}}{1 + (b_i P_i)^{1/m_i}} + \frac{q_j (b_j P_j)^{1/m_j}}{1 + \left(\sum_{j=1}^{N} (b_j P_j)^{1/m_j}\right)} \tag{9}$$

3. Results and discussion

3.1. Characterization

The resulting mass of each treated sample was weighed and compared to that of the pristine sepiolite in order to understand the changes brought about by the acid treatment. The results (Fig. 1) show that there is a mass loss as great as 12% for only two minutes of microwave acid treatment. Sample mass keeps decreasing linearly for increasing time of treatment, at a rate of approximately 1.7 wt.% min^{-1} in the following 14 min. This trend could be related to the progressive transformation from sepiolite to pure silica at an infinitely long acid treatment.

In order to determine the chemical composition of the sepiolite prior and after the microwave-assisted acid treatment, X-ray fluorescence (XRF) analyses were carried out (Fig. 2). As reported in a previous study [35], the mineralogical formula cannot be obtained

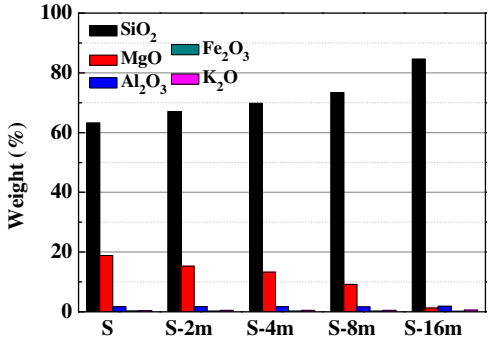

Fig. 2. Chemical composition of sepiolite and modified sepiolites by acid treatment determined by X-ray fluorescence.

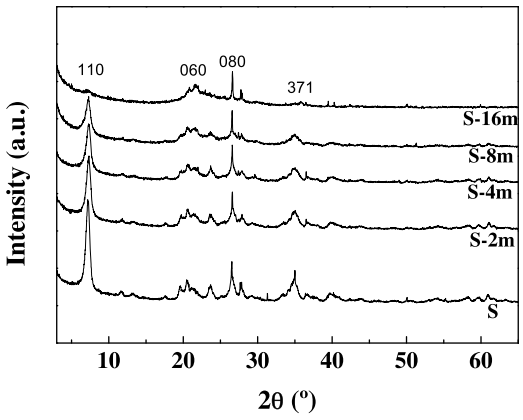

Fig. 3. X ray diffractograms of starting sepiolite and modified sepiolite by acid treatment.

by the coexistence of at least two sepiolite phases and other crystallography phases. The microwave-assisted acid treatment causes a progressive loss of Mg^{2+} species of the octahedral sheet, while Si^{4+} and Al^{3+} are not extracted of the framework (see Fig. 2).

The diffraction pattern of the raw material (Fig. 3) shows that sepiolite is the main mineralogical phase. In addition, a detailed analysis of the diffractogram shows minor amounts of quartz, feldspar and opal CT, as previously reported [35]. The microwave-assisted acid treatment causes significant changes in the diffraction pattern of the sepiolite, mainly in the d_{110} reflection, located at about 2θ = 7.3°. Moreover, the d_{441}, d_{530} and d_{371} reflections located at 2θ between 31.9 and 36.1° are highly sensitive to the acid treatment, leading to a structural transformation by the leaching of Mg^{2+} species, as shown in Fig. 2, and generating a SiO_2-rich and amorphous material after 16 min of acid treatment. In addition, the diffraction peaks attributed to quartz (e.g. reflection at 26° overlapped with the narrow peak assigned to 080 planes) and feldspar (reflections located between 21–22°) [35] seems to remain unaltered by the acid treatment.

The FTIR spectra of the raw sepiolite and the samples treated with HNO_3 and microwave radiation are compiled in Fig. 4. The FTIR spectrum of the raw sepiolite can be analyzed in three subregions. The first set of bands located between 3700 and 3000 cm^{-1} are attributed to the stretching vibrational mode of —OH. Previous research of FTIR has revealed the presence of two bands located at about 3689 and 3633 cm^{-1} assigned to —OH groups coordinated to the magnesium species present in sepiolite [48]. In addition, the band located at about 3564 cm^{-1} is attributed to the water coordinated with the magnesium species of the sepiolite [48]. Other bands located below 3500 cm^{-1} are attributed to zeolitic and coordinated water [49]. The second set of bands is located between 1700 and 1600 cm^{-1} attributed to —OH bending modes. Thus, the bands located at about 1627 and 1666 cm^{-1} are assigned to bending modes of adsorbed water and zeolitic water, respectively [50]. Finally, the bands located in the range of 1300–900 cm^{-1} are assigned to Si—O stretching modes, while the bands located between 900 and 700 cm^{-1} are assigned to M—OH deformation modes and the bands located 700 and 600 cm^{-1} are ascribed to M—OH translation modes [48].

The FTIR spectra of the samples modified with the microwave-assisted acid treatment reveal the progressive loss of the bands attributed to magnesium species coordinated with —OH and H_2O located between 3700 and 3550 cm^{-1}. This decrease is not proportional for all bands, which indicates different reactivity sites under the acid treatment. In addition, the appearance of a new band located at about 3740 cm^{-1} is noticeable and assigned to the —OH stretching vibrational mode in the form of Si—OH [51]. These results

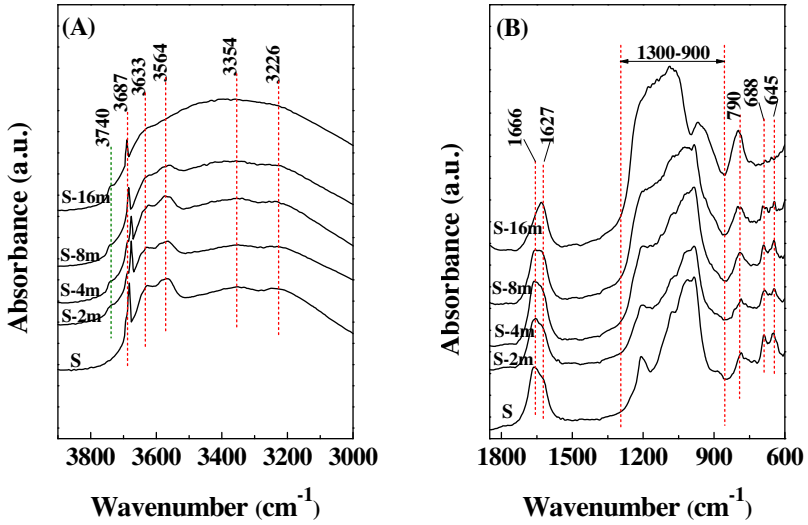

Fig. 4. FTIR spectra for sepiolite and samples treated with HNO_3 and microwave radiation in the region (A) 4000–3000 and (B) 1900–600 cm^{-1}.

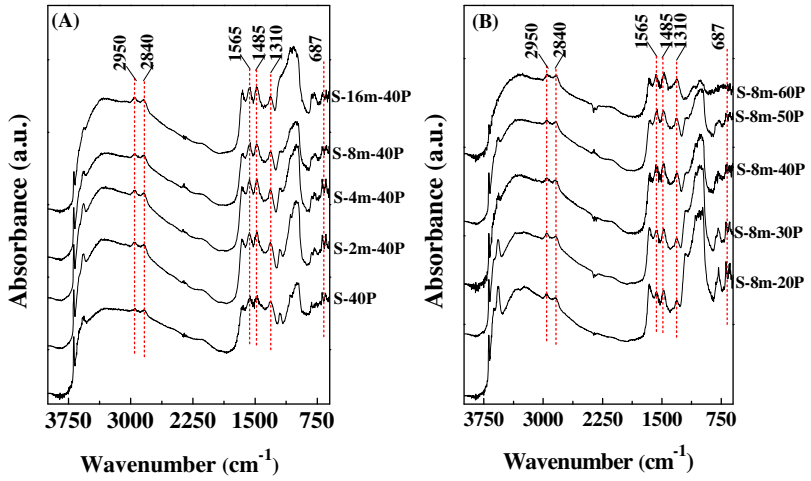

Fig. 5. FTIR spectra for (A) samples impregnated with the same quantity of PEI (40 wt.%) and (B) sample treated with microwave radiation after PEI impregnation in different quantities, from 20 to 60 wt.%.

are in agreement with those shown in the gravimetric analysis, XRF and XRD, where the mass loss is associated to the Mg^{2+} leaching of the sepiolite framework, leading to an almost amorphous silica after 16 min of acid treatment. The H—O—H bending modes (1700–1600 cm^{-1}) reflect the loss of the zeolitic water, located at about 1666 cm^{-1}, which suggests the decrease of microporosity after the acid treatment. The band attributed to Si—O stretching mode is modified, leading to a broad band between 1325 and 1000 cm^{-1}, which confirms the changes of the sepiolite structure during the acid treatment. The bands attributed to M—OH deformation and translation also suffer modifications due to the formation of free silica [51].

Both raw sepiolite and sepiolite treated with acid and microwaves were impregnated with PEI, as amine source (Fig. 5). In all cases, new bands arise at 2950 and 2840 cm^{-1}, attributed to asymmetric and symmetric C—H stretching mode, respectively, due to the alkyl chain of PEI [52]. The bands located at 1565 and 1485 cm^{-1} are attributed to asymmetric and symmetric bending of primary amines, respectively [53], although the band located at 1485 cm^{-1} can be also attributed to the deformation of C—H bond [54]. In addition, the band located about 1310 cm^{-1} is assigned to NCOO- skeletal vibration [53] and the band located about 687 cm^{-1} is attributed to N—H bending vibration of the PEI [55].

N_2 adsorption-desorption isotherms at 77 K are compiled in Fig. 6. According to the IUPAC classification, both raw sepiolite and the sepiolite treated with HNO_3 and microwave radiation display

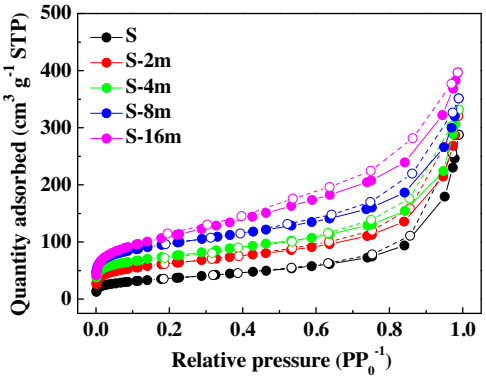

Fig. 6. N_2 adsorption-desorption isotherms at 77 K for sepiolite and sepiolite thermally treated at 2, 4, 8 and 16 min. All samples were outgassed at 473 K.

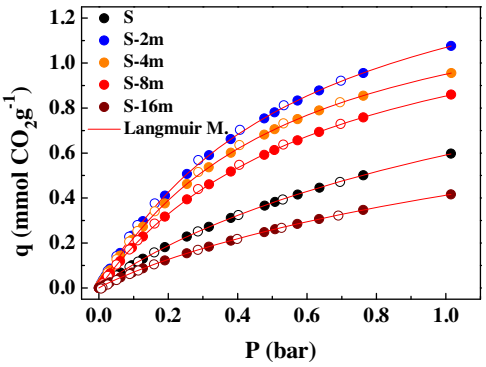

Fig. 7. CO_2 adsorption-desorption isotherms at 298 K. Filled circles for adsorption data and empty for desorption data. Adsorption data were fitted to Langmuir model and curve fit is also plotted (continuous line).

Table 1
Textural properties obtained from N_2 adsorption-desorption isotherms at 77 K for samples outgassed at 473 K.

Sample	S_{BET} ($m^2\ g^{-1}$)	S_{microp} ($m^2\ g^{-1}$)	V_{pore} ($cm^3\ g^{-1}$)	Pore diameter (nm)[a]
$T_{outgass.}$	473 K			
S	128	17	0.38	11.9
S-2 m	206	62	0.43	8.3
S-4 m	296	138	0.46	6.9
S-8 m	366	145	0.56	6.2
S-16 m	433	116	0.66	6.1

[a] Pore diameter calculated by BJH method applied to desorption branch.

a type II isotherm with narrow hysteresis loops, corresponding to H3 type, which is attributed to the presence of narrow slit-shaped pores [56]. The specific surface areas (S_{BET}), pore diameters and pore volumes are compiled in Table 1. The microwave assisted acid treatment produces an increase of the S_{BET} values from 128 $m^2\ g^{-1}$ for the raw sepiolite to 433 $m^2\ g^{-1}$ for the sample treated for 16 min. In addition, the pore volume also increases. This fact is attributed to the formation of cavities by the leaching of Mg^{2+} species coming from centers of octahedral sites of the sepiolite, although this fact-could cause microporosity loss by a framework collapse forlonger treatment with acid [35,57].

The impregnation of sepiolite with PEI induces a dramatic decrease of the surface area and the pore volume due to the stacking of the PEI molecules in micropores and mesopores, which hinders the access of CO_2 molecules to the porous inner structure of the adsorbents.

3.2. CO_2 adsorption

3.2.1. CO_2 adsorption of sepiolites

The CO_2 adsorption-desorption isotherms at 298 K are shown in Fig. 7. Langmuir model was fitted to the adsorption isotherms.

It can be observed that the microwave-assisted acid treatment had a positive effect on CO_2 adsorption, but it tends to progressively decrease CO_2 adsorption capacity at longer treatment periods, probably due to the progressive depletion by leaching of Mg^{2+} cations.

The CO_2 isotherms at 298, 318 and 338 K are shown in Fig. 8. In all cases the equilibrium adsorption capacities decrease markedly with increasing temperature, especially at pressures close to 1 bar. This behavior indicates that the CO_2 adsorption process takes place as a physical process, suggesting the exothermic nature of CO_2 adsorption.

From the CO_2 adsorption isotherms, it can be observed that after two minutes of assisted treatment, the material almost doubles the amount of CO_2 adsorbed at the same studied conditions, reaching 1.07 mmol $CO_2\ g^{-1}$. This result is higher than other data reported in the literature for clay materials, such as intercalated bentonite

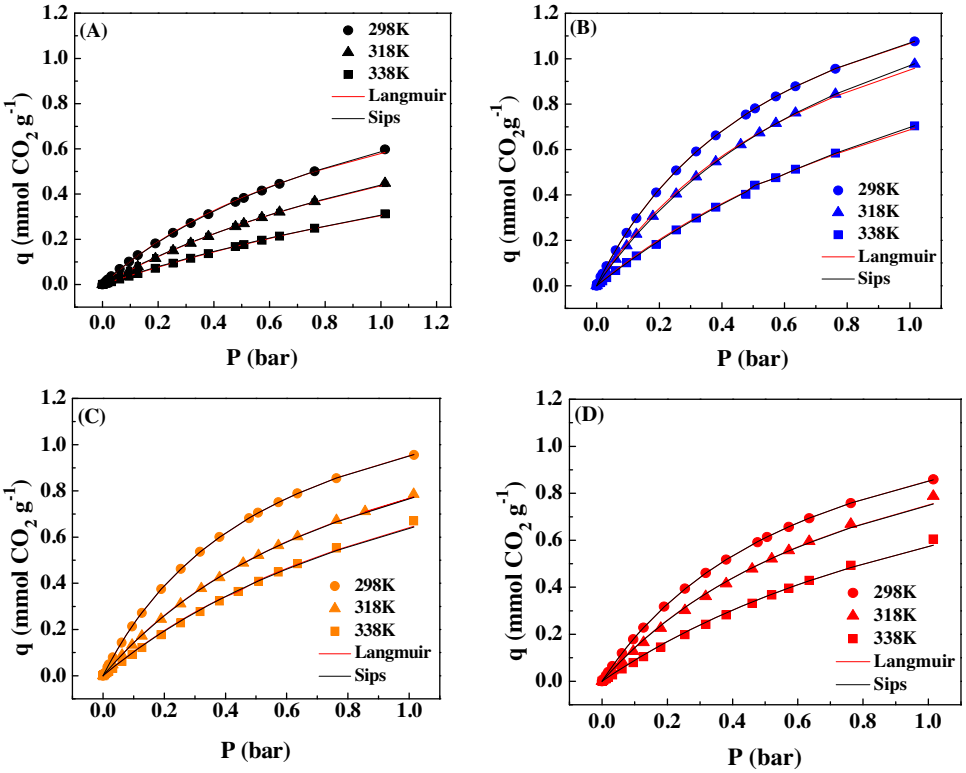

Fig. 8. CO_2 adsorption isotherms at 298 (circle), 318 (triangle) and 338 K (square) for (A) raw sepiolite, (B) S-2 m, (C) S-4 m and (D) S-8 m. Langmuir and Sips fitting data are also plotted as red and black line respectively. (For interpretation of the references to color in this figure legend, the reader is referred to the web version of this article.)

Table 2
Langmuir fit parameterfor S, S-2 m, S-4 m and S-8 m samples. Average of Isosteric heats of adsorption (H_{aver}) in the studied pressure range calculated from Clausius Clapeyron equation are also shown.

	T	Langmuir fit parameters					H_{aver}
		q_m	b	R^2	b_0	E_a	
S	298	1.199	0.937	0.99327	0.000193	21.06	20.88
	318		0.574	0.99538			
	338		0.342	0.99954			
S-2 m	298	1.714	1.654	0.99641	0.000912	18.74	18.95
	318		1.246	0.99942			
	338		0.670	0.99874			
S-4 m	298	1.496	1.755	0.99942	0.001274	17.86	18.84
	318		1.055	0.99899			
	338		0.749	0.99952			
S-8 m	298	1.421	1.504	0.99932	0.001931	16.59	17.69
	318		1.121	0.99995			
	338		0.677	0.99591			

T: Kelvin; q_m: mmol g^{-1}, b and b_0: bar^{-1}, E_a and H_{aver}: kJ mol^{-1}.

Table 3
Sips fit parameterfor S, S-2 m, S-4 m and S-8 m samples.

	T	Sips fit parameters					
		q_m	b	m	R^2	b_0	E_a
S	298	1.393	0.719	1.044	0.99631	0.000171	20.71
	318		0.447		0.99441		
	338		0.266		0.99978		
S-2 m	298	1.736	1.611	1.006	0.99831	0.000898	18.71
	318		1.211		0.99988		
	338		0.653		0.99902		
S-4 m	298	1.479	1.795	0.994	0.99955	0.001914	18.09
	318		1.072		0.99912		
	338		0.758		0.99994		
S-8 m	298	1.404	1.539	0.994	0.99902	0.001951	16.63
	318		1.142		0.99981		
	338		0.692		0.99772		

T: Kelvin; q_m: mmol g^{-1}, b and b_0: bar^{-1}, E_a: kJ mol^{-1}.

MEA [58] and acid-activated bentonite [59] that adsorbed 0.79 and 0.75 mmol CO_2 g^{-1} at 298 K, respectively.

The Langmuir and Sips fitting parameters are summarized in Tables 2 and 3, respectively. In Fig. 9 isosteric heats of adsorption calculated using the Clausius-Clapeyron equation are shown. A decrease in isosteric heats of adsorption with increasing time of acid treatment may be observed. This fact could be related with the amorphization of the sepiolite due to the thermal acid treatment. The depletion of Mg^{2+} species could lead to the decrease of the affinity to CO_2 adsorption due to a minor polarity of sepiolite surface, although the increase of S_{BET} values and pore volume improves CO_2 capacities in the first minutes due to the sepiolite structureis not collapsed yet.

3.2.2. CO_2 adsorption of sepiolite functionalized with PEI

In order to improve the CO_2 adsorption capacity of the sepiolite modified by acid treatment assisted with microwaves, all samples (sepiolite and acid treated sepiolites) were functionalized with the same amount of PEI (40 wt.%) by impregnation following a previously described methodology [18,20].

CO_2 isotherms at 298 K for PEI-sepiolites are shown in Fig. 10. It can be observed that after 2 min of acid treatment the quantity adsorbed remains almost unaltered in comparison to the stating

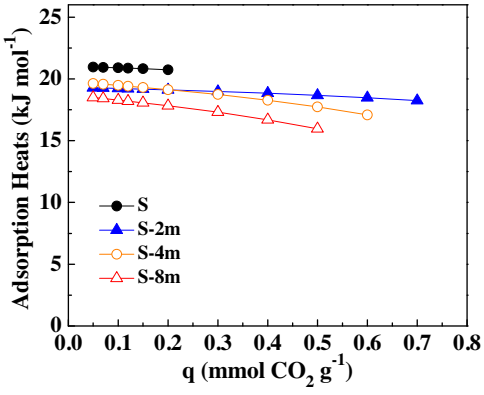

Fig. 9. Isosteric heats of adsorption for S (fill circle), S-2 m (fill triangle), S-4 m (empty circle) and S-8 m (empty triangle) calculated from the Clausius-Clapeyron equation.

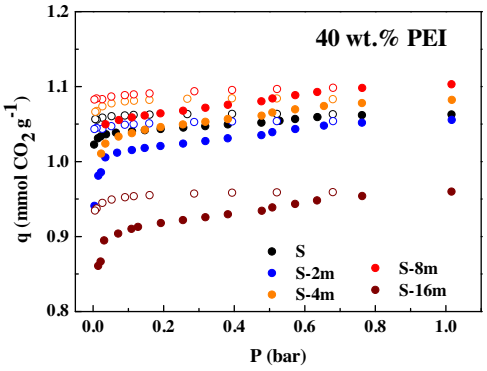

Fig. 10. CO_2 adsorption-desorption isotherms at 298 K for PEI (40 wt.%) impregnated sepiolite and modified sepiolites by acid treatment with microwave radiation. Filled circles for adsorption data and empty for desorption data.

Table 4
Content (%) of C and N determined by elemental analysis related to the amount of CO_2 adsorbed at 298 K and 1 bar.

Sample	Elemental analysis (CNH)		q	mol CO_2/mol N
	C	N		
20% PEI	18.90	12.03	0.66	0.077
30% PEI	26.84	15.26	1.15	0.105
40% PEI	30.12	17.21	1.11	0.090
50% PEI	34.25	19.52	0.97	0.069

q: mmol CO_2 g^{-1}.

Table 5
Quantity of CO_2 adsorbed (mmol CO_2 g^{-1}) at 298 K and 1 bar for PEI impregnated sepiolite (30 and 50 wt.%) modified by acid treatment with microwave radiation after 8 min.

Sample S-8 m	q (mmol CO_2 g^{-1}), P = 1 bar		
	298 K	318 K	338 K
30%PEI	1.12	1.37	1.70
50%PEI	0.89	0.90	1.05

material, however a slight increase is observed after 4 and 8 min of treatment. The high initial slope of the isotherms for samples impregnated with PEI in comparison with the samples without amine groups suggests that these adsorbents are not suitable for PSA processes, where low pressure is required by the regeneration of the adsorbent; however this adsorbent might be appropriate for TSA processes, in which the adsorbent can be regenerated by thermal treatment.

All isotherms showed hysteresis loops associated with the presence of amines. S-8 m sample (40 wt.% PEI) displays the highest CO_2 adsorbed value (1.11 mmol CO_2 g^{-1} at 298 K and 1 bar), and therefore this sample was chosen to evaluate the influence of the PEI impregnated on the sepiolite. Thus, S-8 m sample was also impregnated with 20, 30 and 50 wt.% PEI.

From the elemental analysis data, reported in Table 4, it can be observed how the nitrogen content increases directly with the amount of polymer impregnated. However, higher nitrogen content does not imply larger CO_2 adsorption capacity. In this sense, it has been reported in the literature that large amount of rich-amine polymer are stacked on the surface of the adsorbent decreasing the amount of available amine sites [18]. In the present work, the highest CO_2 adsorption capacity, 1.15 mmol CO_2 g^{-1} at 298 K and 1 bar, is obtained when S-8 m sample is impregnated with 30% PEI, where the nitrogen content is 15.26% N and the efficiency in terms of mol CO_2/mol N is 0.105. The influence of the temperature of the PEI-functionalized materials in the CO_2 adsorption were evaluated at 1 bar for samples impregnated with 30 and 50 wt.% PEI (higher and lower efficiency, respectively) at 298, 318 and 338 K (Table 5).

The highest CO_2 adsorption capacity was obtained for S-8 m sample impregnated with 30 wt.% PEI in the temperature range studied (298–338 K). It is widely reported that CO_2 adsorption is an exothermic process, so increasing temperature is unfavorable for CO_2 adsorption capacity. However, the formation of bulk-like PEI inside the pore (or over the adsorbent surface) leads to an improving of the CO_2 uptake, although this process is limited by diffusion resistance at low temperatures [60]. An increase of the temperature diminishes the diffusion limitation of CO_2through PEI layersleading to higher amount of accessible amine sites [61,62]. It is well reported in the literaturethat the reaction mechanism of $CO_2$with amine groups takes place through zwitterion formation [22,63,64], according to the following reactions:

$$RR'NH + CO_2 \rightarrow RR'NH^+COO^-(\text{Zwitterion}) \quad (1)$$

$$RR'NH^+COO^- + RRNH \leftrightarrow RR'NCOO^-(\text{Carbamate}) + RRNH_2{}^+ \quad (2)$$

The overall reaction is

$$2RR'NH + CO_2 \leftrightarrow RR'NCOO^- + RRNH_2{}^+ \quad (3)$$

$$RR'NCOO^- + H_2O \leftrightarrow RR'NH + HCO_3{}^- \quad (4)$$

The formation of zwitterion is followed by the deprotonation of the zwitterion by a base to produce a carbamate [65,66]. The CO_2 adsorption efficiency, defined as the ratio between moles of CO_2 adsorbed and moles of N in the material, is a useful tool to quantify the effectiveness of amine-based CO_2 adsorbents. In the mechanism of zwitterion formation, under anhydrous conditions, a second amine typically acts as the base to produce an ammonium carbamate, giving a theoretical maximum amine efficiency of 0.5. This suggests that achieving a high density of amines in close proximity to each other can enhance the amine efficiency.

Thereby, from the proposed reaction mechanism of CO_2 with amine groups the maximum efficiency in anhydrous conditions is 0.5 mol CO_2/mol N. The data shown in the current research reveals that the maximum efficiency was found around 0.11 mol CO_2/mol N, calculated by using the maximum quantity of CO_2 adsorbed in site 2 (q_{m2}), adsorbed amount that is related to chemical adsorption. This result is lower than those data reported for other adsorbents such as PEI-SBA-15 [20]. The low efficiency is related with the structure arrangement of sepiolite with slit shaped pores, where PEI layers create a viscous network so that a high quantity of amino groups are inaccessible for CO_2 molecules in the temperature range under study. With regards to adsorbed CO_2, the results obtained in this work are in the range to other data previously reported (see Table 6). Taking into account the wide availability and relatively low cost of sepiolitein comparison to other porous materials, such as SBA-15 or MCM-41, as well as the simplicity of the modification treatment, these adsorbents show promise for CO_2 adsorption applications.

Table 6
Some data of amount of CO_2 adsorbed in PEI-impregnated samples collected from bibliography.

Sample	PEI (wt.%)	S (m^2 g^{-1})	q (mmol g^{-1})	Operation conditions	T (K)	Reference
AC	30	90	1.14	100% CO_2	298	[67]
S-8 m	30	41	1.12	100% CO_2	298	This work
S-8 m	30	41	1.70	100% CO_2	338	This work
Meso Al_2O_3	40	58	1.50	100% CO_2	373	[68]
MCM-41	50	4	0.75	100% CO_2	298	[69]
MCM-41	50	4	2.03	15% CO_2 in N_2	348	[70]
MCM-41	50	4	2.84	13% CO_2 (10% H_2O) in N_2	348	[70]
MCSs	50	36	3.71	15% CO_2 in N_2	348	[71]
AC	50	2	1.30	8% CO_2 in N_2	333	[72]
AC/K_2CO_3	50	4	1.20	8% CO_2 in N_2	333	[72]
SBA-15	50	5	1.60	100% CO_2	348	[73]
UiO66	30	37	1.65	100% CO_2	338	[74]

MCSs: mesoporous carbon spheres.

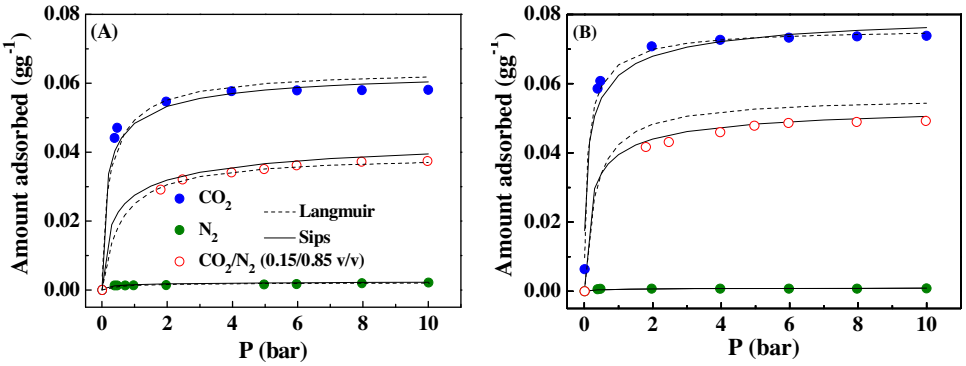

Fig. 11. CO_2 (blue circles), N_2 (green circles) and CO_2/N_2 (15/85 v/v) (empty red circles) experimental isotherms at (A) 298 K and (B) 338 K for 30 wt.% PEI-S-8 m. Extended Sips (line) and Extended Langmuir (dashed line) with Dualsite fit model are also plotted. (For interpretation of the references to color in this figure legend, the reader is referred to the web version of this article.)

Table 7
Dualsite Langmuir parameters for CO_2 and Langmuir parameters for N_2 at 298 and 338 K for S-8 m impregnated with 30% PEI.

T(K)/gas	Site 1		Site 2		R^2	mol CO_2/mol N Site2
	q_m	b	q_m	b		
298/CO_2	0.704	1.556	0.751	12.041	0.96222	0.068
298/N_2	0.077	1.702	–	–	0.83109	
338/CO_2	0.569	2.002	1.159	22.004	0.98491	0.106
338/N_2	0.032	1.661	–	–	0.71928	

q_m: mmol g^{-1}; b: bar^{-1}.

Table 8
Dualsite Sips parameters for CO_2 and Sips parameters for N_2 at 298 and 338 K for S-8 m impregnated with 30% PEI.

T(K)/gas	Site 1			Site 2			R^2	mol CO_2/mol N Site2
	q_m	b	m	q_m	b	m		
298/CO_2	0.768	2.001	1.399	0.704	18.002	1.452	0.94854	0.064
298/N_2	0.085	1.702	1.796	–	–	–	0.91508	
338/CO_2	0.659	1.799	1.397	1.204	22.003	1.804	0.94604	0.111
338/N_2	0.033	1.668	1.121	–	–	–	0.75092	

q_m: mmol g^{-1}; b: bar^{-1}.

Finally, in order to simulate the flue gas conditions, CO_2, N_2 and CO_2/N_2 mixture (15/85% v/v) were obtained in a magnetic suspension balance (Rubotherm, Germany) equipped with a gas dosing unit. The CO_2/N_2 mixture isotherms obtained were adjusted with relatively good accuracy from the estimated Sips parameters for the pure gas isotherms using Extended Sips model with Dualsite model.

In Fig. 11(a) and (b), it may be observed that the presence of amine groups on the adsorbent surface has a direct impact on the shape of CO_2 and N_2 pure isotherms. As previously indicated, CO_2 adsorption on amino-functionalized materials occurs by the Zwitterion mechanism, which is observed in the higher *b* values from Dualsite Langmuir and Dualsite Sips models (see Tables 7 and 8), while N_2 isotherms show a nearly linear behavior indicating lower affinity for these amino functionalized materials.

In order to predict the binary experimental adsorption data, Extended Dualsite Langmuir and Extended Dualsite Sips models were used (Fig. 11). From the monocomponent data, simulated binary isotherms were satisfactorily predicted. The Extended Dualsite Sips model shows higher accuracywith respect to the binary experimental data. This fact is related to the presence of an additional parameterin this model.

In terms of selectivity, the Extended Sips model predicts a decreasing selectivity as pressure increases from 128 (0.3 bar) to 54 (10 bar) mol CO_2/mol N_2 at 298 K. On the other hand, when the temperature increases, the selectivity predicted using the Extended Sips model is higher due to the lower CO_2 diffusion resistances. S-8 m impregnated with 30% of PEI exhibited a high selectivity at 338 K, decreasing from 440 to 240 mol CO_2/mol N_2 (from 0.05 to 1.5 bar of CO_2 partial pressure).

4. Conclusions

The microwave-assisted acid treatment has proved to be an effective method to activate sepiolites. Using this type of treatment, in just a few minutes, it is possible to obtain materials with textural properties similar to those found usingtraditional methods, which require over 48 h of treatment. These acid treated sepiolites with assistance of microwave radiation exhibited a higher CO_2 adsorption capacity than the original material, reaching 47 mg CO_2 g^{-1} at 1 bar and 298 K, probably due to their higher specific surface area and pore volume.

After PEI impregnation, the sample treated for 8 min (S-8 m) shows the best CO_2 capacity. The interaction of CO_2 with the PEI is thermally activated, so that CO_2 retention as well as CO_2/N_2 selectivity increases with the temperature in the studied range (298–338 K), which is desirable in the post-combustion emission scenarios. Thereby the S-8 m sample adsorbed 75 mg CO_2 g^{-1}

(338 K, 1 bar), also showing high CO_2 selectivity over N_2 (440 mol CO_2/mol N_2 at 0.3 bar).

Acknowledgements

We thank project CTQ2015-68951-C3-3-R (Ministerio de Economía y Competitividad, Spain) and FEDER funds, project P12-RNM-1565 (Excelencia, Junta de Andalucía, Spain) and European project295156 FP7-PEOPLE-2011-IRSES for financial support. E. Vilarrasa-Garcia thanks CAPES/PNPD (Brazilian Ministry of Education) for post-doctoral fellowship.

References

[1] M.Z. Jacobson, Review of solutions to global warming, air pollution, and energy security, Energy Environ. Sci. 2 (2009) 148–173.
[2] Climate Change 2014: Mitigation of Climate Change: Contribution of Working Group III to the Fifth Assessment Report of the Intergovernmental Panel on Climate Change, Cambridge University Press, Cambridge, United Kingdom and New York, NY, USA, 2014.
[3] S. Choi, J.H. Drese, C.W. Jones, Adsorbent materials for carbon dioxide capture from large anthropogenic point sources, ChemSusChem 2 (2009) 796–854.
[4] P.V. Danckwerts, The reaction of CO_2 with ethanolamines, Chem. Eng. Sci. 34 (1979) 443–446.
[5] E. Rinker, S.S. Ashour, O.C. Sandall, Absorption of carbon dioxide into aqueous blends of diethanolamine and methyldiethanolamine, Ind. Eng. Chem. Res. 39 (2000) 4346–4356.
[6] S. Ma'mun, H.F. Svendsen, K.A. Hoff, O. Juliussen, Selection of new absorbents for carbon dioxide capture, Energy Convers. Manage. 48 (2007) 251–258.
[7] M. Balsamo, T. Budinova, A. Erto, A. Lancia, B. Petrova, N. Petrov, B. Tsyntsarski, CO_2 adsorption onto synthetic activated carbon: kinetic, thermodynamic and regeneration studies, Sep. Purif. Technol. 116 (2013) 214–221.
[8] J. Schell, N. Casas, D. Marx, M. Mazzotti, Precombustion CO_2 capture by pressure swing adsorption (PSA): comparison of laboratory PSA experiments and simulations, Ind. Eng. Chem. Res. 52 (2013) 8311–8322.
[9] G.D. Pirngruber, D. Leinekugel-le-Cocq, Design of a pressure swing adsorption process for postcombustion CO_2 capture, Ind. Eng. Chem. Res. 52 (2013) 5985–5996.
[10] G.D. Pirngruber, F. Guillou, A. Gomez, M. Clausse, A theoretical analysis of the energy consumption of post-combustion CO_2 capture processes by temperature swing adsorption using solid sorbents, Int. J. Greenh. Gas Control 14 (2013) 74–83.
[11] J.P. Sculley, W.N. Verdegaal, W. Lu, M. Wriedt, H.C. Zhou, High-throughput analytical model to evaluate materials for temperature swing adsorption processes, Adv. Mater. 25 (2013) 3957–3961.
[12] S. Datta, M.P. Henry, Y.J. Lin, A.T. Fracaro, C.S. Millard, S.W. Snyder, Electrochemical CO_2 capture using resin-wafer electrodeionization, Ind. Eng. Chem. Res. 52 (2013) 15177–15186.
[13] Q. Huang, M. Eic, Commercial adsorbents as benchmark materials for separation of carbon dioxide and nitrogen by vacuum swing adsorption process, Sep. Purif. Technol. 103 (2013) 203–215.
[14] Y.H. Kim, D.G. Lee, D.K. Moon, S.H. Byeon, H.W. Ahn, C.H. Lee, Effect of bed void volume on pressure vacuum swing adsorption for air separation, Korean J. Chem. Eng. 31 (2014) 132–141.
[15] A. Goeppert, M. Czaun, R.B. May, G.K.S. Prakash, G.A. Olah, S.R. Narayanan, Carbon dioxide capture from the air using a polyamine based regenerable solid adsorbent, J. Am. Chem. Soc. 133 (2011) 20164–20167.
[16] J. Zhang, R. Singh, P.A. Webley, Alkali and alkaline-earth cation exchanged chabazite zeolites for adsorption based CO_2 capture, Microporous Mesoporous Mater. 111 (2008) 478–487.
[17] N. Hiyoshi, K. Yogo, T. Yashima, Adsorption characteristics of carbon dioxide on organically functionalized SBA-15, Microporous Mesoporous Mater. 84 (2005) 357–365.
[18] R. Sanz, G. Calleja, A. Arencibia, E.S. Sanz-Perez, CO_2 adsorption on branched polyethyleneimine-impregnated mesoporous silica SBA-15, Appl. Surf. Sci. 256 (2010) 5323–5328.
[19] E. Vilarrasa-García, J.A. Cecilia, S.M.L. Santos, C.L. Cavalcante Jr., J. Jiménez-Jiménez, D.C.S. Azevedo, E. Rodríguez-Castellón, CO_2 adsorption on APTES functionalized mesocellular foams obtained from mesoporous silicas, Microporous Mesoporous Mater. 187 (2014) 125–134.
[20] E. Vilarrasa-García, E.M. Ortigosa-Moya, J.A. Cecilia, C.L. Cavalcante Jr., J. Jiménez-Jiménez, D.C.S. Azevedo, E. Rodríguez-Castellón, CO_2 adsorption on amine modified mesoporous silicas: effect of the progressive disorder of the honeycomb arrangement, Microporous Mesoporous Mater. 209 (2015) 172–183.
[21] L. Wang, R.T. Yang, Increasing selective CO_2 adsorption on amine-grafted SBA-15 by increasing silanol density, J. Phys. Chem. C 115 (2011) 21264–21272.
[22] M.R. Mello, D. Phanon, G.Q. Silveira, P.L. Llewellyn, C.H. Ronconi, Amine-modified MCM-41 mesoporous silica for carbon dioxide capture, Microporous Mesoporous Mater. 143 (2011) 174–179.
[23] C. Chen, W.J. Son, K.S. You, J.W. Ahn, W.S. Ahn, Carbon dioxide capture using amine-impregnated HMS having textural mesoporosity, Chem. Eng. J. 161 (2010) 46–52.
[24] J.A. Cecilia, E. Vilarrasa-Garcia, C. Garcia-Sancho, R.M.A. Saboya, D.C.S. Azevedo, C.L. Cavalcante Jr., E. Rodríguez-Castellón, Functionalization of hollow silica microspheres by impregnation or grafted of amine groups for the CO_2 capture, Int. J. Greenh. Gas Control 52 (2016) 344–356.
[25] Y. Liu, J. Shi, J. Chen, Q. Ye, H. Pan, Z. Shao, Y. Shi, Dynamic performance of CO_2 adsorption with tetraethylenepentamine-loaded KIT-6, Microporous Mesoporous Mater. 134 (2010) 16–21.
[26] H. Kassab, M. Maksoud, S. Aguado, M. Pera-Titus, B. Albela, L. Bonneviot, Polyethylenimine covalently grafted on mesostructured porous silica for CO_2 capture, RSC Adv. 2 (2012) 2508–2516.
[27] J.R. Li, Y. Ma, M.C. McCarthy, J. Sculley, J. Yu, H.K. Jeong, P.B. Balbuena, H.C. Zhou, Carbon dioxide capture-related gas adsorption and separation in metal-organic frameworks, Coord. Chem. Rev. 255 (2011) 1791–1823.
[28] K. Sumida, D.L. Rogow, J.A. Mason, T.M. McDonald, E.D. Bloch, Z.R. Herm, T.H. Bae, J.R. Long, Carbon dioxide capture in metal–organic frameworks, Chem. Rev. 112 (2012) 724–781.
[29] F.C. Yu, N. Phalak, Z. Sun, L.S. Fan, Activation strategies for calcium-based sorbents for CO_2 capture: a perspective, Ind. Eng. Chem. Res. 51 (2012) 2133–2142.
[30] W. Wang, J. Xiao, X. Wei, J. Ding, X. Wang, C. Song, Development of a new clay supported polyethylenimine composite for CO_2 capture, Appl. Energy 113 (2014) 334–341.
[31] Y.H. Chen, D.L. Lu, Amine modification on kaolinites to enhance CO_2 adsorption, J. Colloid Interface Sci. 436 (2014) 47–51.
[32] C. Chen, D.W. Park, W.S. Ahn, Surface modification of a low cost bentonite for post-combustion CO_2 capture, Appl. Surf. Sci. 283 (2013) 699–704.
[33] E.A. Roth, S. Agarwal, R.K. Gupta, Nanoclay-based solid sorbents for CO_2 capture, Energy Fuel 27 (2013) 4129–4136.
[34] M. Irani, M. Fan, H. Ismail, A. Tuwati, B. Dutcher, A.G. Russell, Modified nanosepiolite as an inexpensive support of tetraethylenepentamine for CO_2 sorption, Nano Energy 11 (2015) 235–246.
[35] F. Franco, M. Pozo, J.A. Cecilia, M. Benítez-Guerrero, E. Pozo, J.A. Martín Rubí, Microwave assisted acid treatment of sepiolite: the role of composition and crystallinity, Appl. Clay Sci. 102 (2014) 15–27.
[36] B. Tyagi, C.D. Chudasama, R.V. Jasra, Characterization of surface acidity of an acid montmorillonite activated with hydrothermal, ultrasonic and microwave techniques, Appl. Clay Sci. 31 (2007) 16–28.
[37] I. Vicente, P. Salagre, Y. Cesteros, Ni nanoparticles supported on microwave-synthesised hectorite for the hydrogenation of styrene oxide, Appl. Catal. A: Gen. 408 (2011) 31–37.
[38] S. Brunauer, P.H. Emmett, E. Teller, Adsorption of gases in multimolecular layers, J. Am. Chem. Soc. 60 (1938) 309–319.
[39] J.H. De Boer, B.C. Lippens, B.G. Linsen, J.C.P. Broekhoff, A. van den Heuvel, T.J. Osinga, The t-curve of multimolecular N_2 adsorption, J. Colloid Interface Sci. 21 (1966) 405–414.
[40] E.P. Barrett, L.G. Joyner, P.P. Halenda, The determination of pore volume and area distributions in porous substances. I. Computations from nitrogen isotherms, J. Am. Chem. Soc. 61 (1951) 373–380.
[41] S. Korichi, A. Elias, A. Mefti, Characterization of smectite after acid activation with microwave irradiation, Appl. Clay Sci. 42 (2009) 432–438.
[42] R. Span, W. Wagner, A new equation of state for carbon dioxide covering dioxide the fluid region from the triple-point temperature to 1100 K at pressures up to 800 MPa, J. Phys. Chem. Ref. Data 25 (1996) 1509–1596.
[43] R. Span, E.W. Lemmon, R.T. Jacobsen, W. Wagner, A.A. Yokozeki, A reference equation of state for the thermodynamic properties of nitrogen for temperatures from 63.151 to 1000 K and pressures to 2200 MPa, J. Phys. Chem. Ref. Data 29 (2000) 1361–1433.
[44] R.D. McCarty, V.D. Arp, A new wide range equation of state for helium, Adv. Cryog. Eng. 35 (1990) 1465–1475.
[45] F. Dreisbach, R. Staudt, J.U. Keller, High pressure adsorption data of methane, nitrogen, carbon dioxide and their binary and ternary mixtures on activated carbon, Adsorption 5 (1999) 215–227.
[46] F. Rouquerol, J. Rouquerol, K.S.W. Sing, Adsorption by Powders and Porous Solids, Academic Press, 2016, pp. 1999.
[47] D.D. Do, Adsorption Analysis: Equilibria and Kinetics, Imperial College Press, 1998.
[48] R.L. Frost, O.B. Locos, H. Ruan, J.T. Kloprogge, Near-infrared and mid-infrared spectroscopic study of sepiolites and palygorskites, Vib. Spectrosc. 27 (2001) 1–13.
[49] R.L. Frost, G.A. Cash, J.T. Kloprogge, Rocky Mountain leather': sepiolite and attapulgite—an infrared emission spectroscopic study, Vib. Spectrosc. 16 (1998) 173–184.
[50] H.W. Van Der Marel, H. Beutelspacher, Atlas of Infrared Spectroscopy of Clay Minerals and Their Admixtures, Elsevier, New York, 1976.
[51] J. Madejová, J. Bujdák, M. Janek, P. Komadel, Comparative FT-IR study of structural modifications during acid treatment of dioctahedral smectites and hectorite, Spectrochim. Acta A: Mol. Biomol. Spectrosc. 54 (1998) 1397–1406.
[52] T.C. Drage, A. Arenillas, K.M. Smith, C.E. Snape, Thermal stability of polyethylenimine based carbon dioxide adsorbents and its influence on selection of regeneration strategies, Microporous Mesoporous Mater. 116 (2008) 504–512.
[53] X. Wang, V. Schwartz, J.C. Clark, X. Ma, S.H. Overbury, X. Xu, C. Song, Infrared study of CO_2 sorption over molecular basket sorbent consisting of

polyethylenimine-modified mesoporous molecular sieve, J. Phys. Chem. C 113 (2009) 7260–7268.
[54] S. Lakard, G. Herlem, B. Lakard, B. Fahys, Theoretical study of the vibrational spectra of polyethylenimine and polypropylenimine, J. Mol. Struct.: THEOCHEM 685 (2004) 83–87.
[55] L. Han, J.F. Ruan, Y.S. Li, O. Terasaki, S.A. Che, Synthesis and characterization of the amphoteric amino acid bifunctional mesoporous silica, Chem. Mater. 19 (2007) 2860–2867.
[56] K.S.W. Sing, D.H. Everett, R.A.W. Haul, L. Moscou, R.A. Pierotti, J. Rouquerol, T. Siemieniewska, Reporting physisorption data for gas/solid systems with special reference to the determination of surface area and porosity (Recommendations 1984), Pure Appl. Chem. 57 (1985) 603–619.
[57] M.A. Vicente-Rodríguez, J. López-González, M.A. Bañares-Muñoz, Acid activation of a spanish sepiolite: physicochemical characterization, free silica content and surface area of products obtained, Clay Miner. 29 (1994) 361–367.
[58] A.E.I. Elkhalifah, M.A. Bustam, A.M. Shariff, T. Murugesan, Selective adsorption of CO_2 on a regenerable amine-bentonite hybrid adsorbent, Appl. Clay Sci. 107 (2015) 213–219.
[59] C. Volzone, Retention of pollutant gases: comparison between clay minerals and their modified products, Appl. Clay Sci. 36 (2007) 191–196.
[60] A. Sayari, Y. Belmabkhout, R. Serna-Guerrero, Flue gas treatment via CO_2 adsorption, Chem. Eng. J. 171 (2011) 760–774.
[61] A. Heydari-Gorji, A. Sayari, CO_2 capture on polyethylenimine-impregnated hydrophobic mesoporous dilica: experimental and kinetic modeling, Chem. Eng. J. 173 (2011) 72–79.
[62] G. Qi, Y. Wang, L. Estevez, X. Duan, N. Anako, A.H.A. Park, W. Li, C.W. Jones, E.P. Giannelis, High efficiency nanocomposite sorbents for CO_2 capture based on amine-functionalized mesoporous capsules, Energy Environ. Sci. 4 (2011) 444–452.
[63] M. Caplow, Kinetics of carbamate formation and breakdown, J. Am. Chem. Soc. 90 (24) (1968) 6795–6803.
[64] A. Sayari, Y. Belmabkhout, Stabilization of amine-containing CO_2 adsorbents: dramatic effect of water vapor, J. Am. Chem. Soc. 132 (2010) 6312–6314.
[65] L.A. Darunte, K.S. Walton, D.S. Sholl, C.W. Jones, CO_2 capture via adsorption in amine-functionalized sorbents, Curr. Opin. Chem. Eng. 12 (2016) 82–90.
[66] S.A. Didas, M.A. Sakwa-Novak, G.S. Foo, C. Sievers, C.W. Jones, Effect of amine surface coverage on the co-adsorption of CO_2 and water: spectral deconvolution of adsorbed species, J. Phys. Chem Lett. 5 (2014) 4194–4200.
[67] M.G. Plaza, C. Pevida, A. Arenillas, F. Rubiera, J.J. Pis, CO_2 capture by adsorption with nitrogen enriched carbons, Fuel 86 (2007) 2204–2212.
[68] M.G. Plaza, C. Pevida, B. Arias, J. Fermoso, A. Arenillas, F. Rubiera, J.J. Pis, Application of thermogravimetric analysis to the evaluation of aminated solid sorbents for CO_2 capture, J. Therm. Anal. Calorim. 92 (2008) 601–606.
[69] X. Xu, C. Song, J.M. Andresen, B.G. Miller, A.W. Scaroni, Novel polyethylenimine-modified mesoporous molecular sieve of MCM-41 type as high capacity adsorbent for CO_2 capture, Energy Fuels 16 (2002) 1463–1469.
[70] X. Xu, C. Song, B.G. Miller, A.W. Scaroni, Influence of moisture on CO_2 separation from gas mixture by a nanoporous adsorbent based on polyethylenimine-modified molecular sieve MCM-41, Ind. Eng. Chem. Res. 44 (2005) 8113–8119.
[71] M. Wang, L. Ya, J. Wang, Z. Zhang, W. Qiao, D. Long, L. Ling, Adsorption and regeneration study of polyethylenimine-impregnated millimeter-sized mesoporous carbon spheres for post-combustion CO_2 capture, Appl. Energy 168 (2016) 282–290.
[72] Y. Guo, C. Zhao, C. Li, S. Lu, Application of PEI–K_2CO_3/AC for capturing CO_2 from flue gas after combustion, Appl. Energy 129 (2014) 17–24.
[73] N. Gargiulo, A. Peluso, P. Aprea, F. Pepe, D. Caputo, CO_2 adsorption on polyethylenimine-functionalized SBA-15 mesoporous silica: isotherms and modeling, J. Chem. Eng. Data 59 (2014) 896–902.
[74] S. Xian, Y. Wu, J. Wu, X. Wang, J. Xiao, Enhanced dynamic CO_2 adsorption capacity and CO_2/CH_4 selectivity on polyethylenimine-impregnated UiO-66, Ind. Eng. Chem. Res. 54 (2015) 11151–11158.